Journal of Molecular Liquids 381 (2023) 121791

Contents lists available at ScienceDirect

Journal of Molecular Liquids

journal homepage: www.elsevier.com/locate/molliq

Decorated crown ethers as selective ion traps: Solvent's role in crown's preference towards a specific ion

Marijana Hercigonja, Branislav Milovanović, Mihajlo Etinski, Milena Petković *

University of Belgrade – Faculty of Physical Chemistry, Studentski trg 12-16, 11158 Belgrade, Serbia

ARTICLE INFO

Article history:
Received 19 December 2022
Revised 27 March 2023
Accepted 1 April 2023
Available online 6 April 2023

Keywords:
Alkali ion detection
Alkali ion coordination
Crown ethers
Water purification

ABSTRACT

Deviation of sodium and potassium concentrations from their optimal values in living organisms is associated with severe health conditions, thus their precise determination in blood samples requires design of sensitive sensors. Additionally, excess of the two alkali cations should be removed from drinking water. Crown ethers are well-known metal ion traps, as careful choice of crown's size and its substituents might tune it towards favoring a specific ion. It has been proved experimentally that dibrominated bithiophene crown ethers with five and six oxygen atoms selectively capture the Na^+ and the K^+ ion, respectively (Giovannitti et al., Adv. Funct. Mater. 26, 2016, 514) in acetonitrile solution. In the present contribution, we analyzed the nature of ion–crown, ion–solvent, and crown–solvent interactions, and demonstrated that the solvent molecules are responsible for the decorated crown's preference for a particular alkali cation. While past research focused on the ring size and the ion radius compatibillity, which is important for a formation of a stable ion–crown complex, our findings highlight the decisive role of solvent molecules in the selectivity of crown ethers toward particular cations.

1. Introduction

Presence of specific metal ions in particular concentration ranges is essential for a series of complex physiological processes in living cells [1]. Optimal intracellular/extracellular concentrations of Na^+ and K^+ ions, the two most abundant metal cations in the human body, are estimated to be around 12/145 and 150/4.5 mM, respectively [2]. Deficiency or excess of one or both of these alkali cations may cause weakness, dizziness, headache, nausea, vomiting, diarrhea, but is also responsible for more severe conditions, like increased blood pressure, muscle disfunction, hormonal disorders, cardiac arrhythmias (even cardiac arrest), kidney diseases, mental confusion, lethargy, to name a few [3]. Therefore, precise determination of sodium and potassium ions is relevant for health monitoring. Additionally, as high concentration of either of the two ions in drinking water might result in ion imbalance, special attention must be paid to water purification and removal of sodium and potassium cations' excess.

Ion detection is often performed by their capture using functionalized polymers, and subsequent measurement of the electrochemical [4–7] or optical response [8–18]. Optical sensors contain an ionophore which catches the desired ion, and a chromophore capable of efficient light absorption in the UV/VIS spectral range. Depending on the nature of the chromophore and the ionophore, ion binding causes different changes of spectral properties, as it can induce a significant change in the band intensity (on–off switches) [8–12], or lead to a pronounced spectral shift (ratiometric probes) [12–18].

Crown ethers [19] have been proved to be suitable alkali metal cation traps [20–27]. As the negatively charged oxygen atoms attract positively charged metal ions, the strength of the host–guest interaction is predominantly governed by the size and the shape of the crown compound and the ion's radius: the dimensions of the ring and the guest should be such that complexation does not significantly distort host's structure [28]. Three types of complexes have been identified so far.

(*i*) If the size of crown's cavity is large enough to accommodate the cation (the so-called hole-size selectivity [29]) the ion settles close to the center of the crown, which enables its maximum coordination with the oxygen atoms. 15-crown-5 and 18-crown-6 ethers fulfill this condition for Na^+ and K^+, respectively [30,31,11,32,16,6,17]. In this case, the crown's brim and the cation can roughly be treated as being two-dimensional. Recent research has proved that structural dynamics of the snatched guest also affects host's selectivity

* Corresponding author.
E-mail address: milena@ffh.bg.ac.rs (M. Petković).

https://doi.org/10.1016/j.molliq.2023.121791
0167-7322/

[27], as does functionalization of the crown itself (presence of electron withdrawing/donating groups, or aromatic rings) [7].

(*ii*) If the ion is too large to fit in the ring cavity, it places itself between two crowns, thus forming a sandwich structure [10,32,14]. This is the case with 12-crown-4 and Na^+, but also with 15-crown-5 and K^+. In both complexes, the ratio cation:crown equals 1:2 (both crowns' oxygen atoms coordinate with the cation).

(*iii*) If the crown is too large compared to the ion's radius, the crown twists and forms a pocket – an ideal spot for the positively charged particle. This complex is known in the literature as enclosed, or wraparound structure [33,34]. Misaizu and coworkers [34] have recently demonstrated that Na^+ forms both open and closed structures with dibenzo-30-crown-10, whereas dibenzo-30-crown-10 completely encloses K^+.

In all the above cases, the cation maximizes its coordination with the crown's electronegative atoms. The importance of host's and guests's geometric properties for a formation of a stable crown–ion complex was thoroughly investigated (see, for example, reference [28] and references therein). When the crown is not large enough to form a wraparound structure, the solvent molecules provide sufficient coordination for the cation. To the best of our knowledge, a detailed theoretical analysis of the relevance of solvant molecules in crowns' preference towards specific ions has so far not been performed.

Recently, Giovannitti et al. demonstrated that dibrominated bithiophene crown ethers 17-(Crown-5) T2 and 20-(Crown-6) T2 favor the sodium and the potassium ion, respectively, in acetonitrile solutions [11]. The experimental results show that both Crown-5 and Crown-6 bind both cations, whereas inclusion of the brominated bithiophene rings results in a pronounced preference of the smaller/larger crown for the smaller/larger cation. Structural changes induced in the crown by the captured ion were addressed and the properties of the HOMO orbitals of the crown and the complex were studied at the B3LYP/6-31G(d) level, which enabled explanation of notable spectral changes upon ion binding. In the present contribution, we focus on the importance of ion–solvent interaction, and on unraveling the reasons behind the noted selectivity of 17-(Crown-5) T2 (17C5T2) and 20-(Crown-6) T2 (20C6T2) towards Na^+ and K^+, respectively. The paper is organized as follows. Computational details are given in the next Section. The following Section contains results and discussion of quantum chemical and density functional theory-based molecular dynamics simulations of crown ether complexes with the two ions studied in the gas phase, using implicit solvent, as well as with explicit solvent molecules. The paper is summarized in the final Section.

2. Computational details

Quantum chemical calculations were performed using the Gaussian program package [35] at M06-2X/6–311+G(d,p) level [36–41] by employing an ultrafine integration grid. The implicit solvent was included through the Polarizable Continuum Model [42] as implemented in the Gaussian suite of programs.

Density functional theory-based molecular dynamics (DFT-MD) simulations were performed using the BLYP functional [43,44] along with Grimme's D3 correction for dispersion interactions [45]. The electron density was expanded within the mixed Gaussian and plane waves method [46]. DZVP basis set [47] was employed for valence electrons in conjunction with Goedecker-Teter-Hutter type pseudopotentials [48] for core electrons. The plane waves included in the calculations were expanded up to the cutoff energy of 400 Ry. The structures of the model systems M17C5C2 and M20C6C2 will be discussed in Section 3.1. The complexes $[M17C5C2K]^+$/$[M17C5C2Na]^+$ and $[M20C6C2K]^+$/$[M20C6C2Na]^+$ were solvated with 71 and 75 acetonitrile molecules, respectively. Periodic boundary conditions were applied using orthorhombic unit cells with the lengths of 22.936, 13.925, 19.186 Å and 23.093, 17.318, 19.317 Å along the x, y, z axes for the $[M17C5C2K]^+$/$[M17C5C2Na]^+$ and $[M20C6C2K]^+$/$[M20C6C2Na]^+$ solutes, respectively. All simulations were carried out under the NVT ensemble, i.e. thermalized to the temperature of 300 K using CSVR thermostat [49] with the time constant of 100 fs. All systems were equilibrated for 2 ps while production runs lasted 10 ps for all systems. Prior to the DFT-MD simulations, the systems were prepared using force-field molecular dynamics in order to determine the sufficient number of solvent molecules required for a reliable description of the first and the second solvation shell. Simulation box size, initial geometry and velocities of the solvent molecules were determined from the force field NPT molecular dynamics simulation, while atom positions in the crown ether–ion complexes were fixed to preserve their geometries obtained at the DFT level. AmberTools20 [50] software was used to generate topologies with GAFF2 [51] and the AM1-BCC atomic charges for the solutes, and a six-site model force-field for acetonitrile [52]. In all molecular dynamics simulations classical equations of motions were integrated using a timestep of 0.5 fs. All molecular dynamics calculations were carried out using CP2K [53].

One of the drawbacks of standard force field simulations is a lack of precise treatment of atomic charges and polarization upon geometry changes [54,55]. Krimm and coworkers [56] used spectroscopically determined force fields in order to incorporate charge and polarizability fluxes. Jensen and coworkers [57] analyzed around 900 conformations of amino acid peptide models, and demonstrated importance of charge fluxes upon changes of all internal degrees of freedom: bond elongation, angle deformation, and torsion. Popelier and coworkers [58] designed a FFLUX water model by employing the machine learning method kriging in conjunction with the IQA methodology and proved that charge-quadrupole, dipole–dipole, and quadrupole-charge interactions have strong influence on structuring of the water molecules. Moreover, inclusion of multiple moments up to hexadecapole is enabled in the DL_FFLUX model [59]. These models are able to faithfully reproduce dynamics of real systems (for example a few thousand water molecules) on a nanosecond time scale.

The models that we used are based on fixed charges and polarizabilities. We will address this issue in Section 3.4.

2.1. Interacting Quantum Atoms

The Interacting Quantum Atoms [60,61] (IQA) methodology enables electronic energy partitioning. It rests on the Quantum Theory of Atoms in Molecules [62–64] according to which an atom represents a region in space enclosed by a surface of zero flux in the electron density. IQA approach has so far been employed for analysis of various systems with non-covalent interactions [65–81]. Interacting Quantum Fragments (IQF) is a variant of the IQA approach, in which interaction among fragments is analyzed, with the fragments $\mathscr{F}$ being formed by combining appropriate atoms. In this contribution, we will consider three types of fragments: (*i*) the crown ether, (*ii*) the alkali ion, and (*iii*) the solvent molecules (each solvent molecule represents one fragment). We will employ a slightly modified version of the standard IQA methodology, which is thoroughly described in reference [75], according to which the IQA binding energy is defined with respect to the optimized fragments (in the original formulation, the reference geometries are the structures fragments adopt in the complex). It also includes a

definition of the term E_{pro}, as will be explained in the following. The binding energy E_{IQA} between an arbitrary number of fragments $\mathscr{F}_I$ consists of three terms: deformation, promotion, and interaction energy:

$$E_{IQA} = E_{def} + E_{pro} + E_{int}. \quad (1)$$

Deformation energy of a fragment $E_{def}^{\mathscr{F}_I}$ represents the energy required to distort it from its optimized structure into the final geometry it adopts within the complex [75]. The sum of deformation energies of all fragments yields an overall deformation energy E_{def}:

$$E_{def} = \sum_I E_{def}^{\mathscr{F}_I}. \quad (2)$$

It is positive for the crown and the solvent molecules, while it equals zero for the two cations, as they are monoatomic.

Fragment's promotion energy $E_{pro}^{\mathscr{F}_I}$ describes energy changes of the distorted fragment induced by the presence of other fragments. The overall promotion energy E_{pro} is computed according to:

$$E_{pro} = \sum_I E_{pro}^{\mathscr{F}_I}. \quad (3)$$

The interaction energy between two fragments is estimated by considering the interaction between each pair of atoms (i and j) that constitute the two fragments ($\mathscr{F}_I$ and $\mathscr{F}_J$):

$$E_{int}^{\mathscr{F}_I\mathscr{F}_J} = 1/2 \sum_{i\in\mathscr{F}_I} \sum_{j\in\mathscr{F}_J} V_{inter}^{ij}. \quad (4)$$

In the above expression, V_{inter}^{ij} stands for the interaction energy between atoms i and j, which represents a sum of the electrostatic interaction V_{cl}^{ij} and the exchange–correlation term V_{xc}^{ij}. Thus, interaction energy between fragments can also be decomposed into its classical and non-classical component:

$$E_{int}^{\mathscr{F}_I\mathscr{F}_J} = E_{cl}^{\mathscr{F}_I\mathscr{F}_J} + E_{xc}^{\mathscr{F}_I\mathscr{F}_J}. \quad (5)$$

The overall binding energy between all fragments is thus given by:

$$E_{IQA} = \sum_I \left(E_{def}^{\mathscr{F}_I} + E_{pro}^{\mathscr{F}_I}\right) + 1/2 \sum_I \sum_J E_{int}^{\mathscr{F}_I\mathscr{F}_J}. \quad (6)$$

The IQA analysis in this work was carried out using the AIMAll software [82].

3. Results and discussion

3.1. Optimized geometries and binding energies

Optimized structures of the two decorated crown ethers in the gas phase are depicted in Fig. 1, Panels A and C. It was previously noted that crown ethers display geometric selectivity, i.e. favor metal ions with optimal dimensions for settling in the middle of crowns without causing significant ring distortion [28]. One would, thus, expect the 17C5T2/20C6T2 crown to display preference towards Na^+/K^+. The structures of the four optimized complexes $[17C5T2Na]^+$, $[17C5T2K]^+$, $[20C6T2Na]^+$, and $[20C6T2K]^+$ in the gas phase are presented in Fig. 2, and the corresponding binding energies are summarized in Table 1. As expected, the sodium ion is located in the center of both rings, as is the potassium ion in the $[20C6T2K]^+$ complex, whereas, K^+ is located outside the 17C5T2 ring. The computed binding energies in the gas phase are misleading, as they suggest that both crowns display significantly stronger interaction with Na^+. The results obtained by reoptimizing the four structures in implicit solvent (acetonitrile was used as a solvent, in accord with the experiments described in reference [11]) suggest that both crowns slightly favor the larger ion. The implicit solvent decreases binding energies by up to almost 75 kcal/mol, which implies that the solvent plays a very important role in stabilizing the complexes, and subsequently in the ion trapping process, so it cannot be neglected. The computed binding energies, however, do not explain the reason behind the experimentally demonstrated selectivity of the two crowns. Thus, we went a step further and included a limited number of explicit solvent molecules.

3.2. Alkali ion coordination

The four optimized crown–ion geometries, Fig. 2, can be used as initial structures for optimization of (complexed ion)-solvent clusters. Ideally, one would surround the complex with a sufficient number of solvent molecules in order to include the first and the second solvation shell. However, such computations using density functional theory with hybrid meta GGA functionals alone are extremely computationally demanding. Therefore, we decided to include only solvent molecules that interact directly with the captured ion. The question is – how many solvent molecules interact with each ion in each complex? Before we tackle this problem, let us introduce a simplified model for solvent molecules. As already mentioned, the experiments which demonstrated that the two crown ethers favor different cations were performed in acetonitrile [11]. The solvent molecules are expected to be oriented with the negative ends (the nitrogen atoms) toward cations. As the methyl groups do not directly interact with the ions, they might be substituted with hydrogen atoms. This simplification would modestly decrease the number of electrons in quantum chemical calculations, but more importantly, dealing with the rotation of the methyl groups would be avoided. In order to verify that acetonitrile molecules can safely be replaced with the suggested model, we optimized the structures of acetonitrile (AN) and hydrogen cyanide (HCN) and performed QTAIM analysis using the AIMAll software [82]. The Bader charges[63] of the nitrogen/carbon atom in AN and HCN amount to −1.195/0.925 and −1.145/0.947, respectively. Furthermore, the corresponding C–N distances in AN and HCN equal 1.148 and 1.145Å. Nitrogen and carbon atomic dipole moments in the two systems are presented in Table 2. The intra-atomic dipole moments μ_{intra}^{atom}, which result from atom polarization [83] are only slightly larger in HCN. The total dipole of the nitrogen atom is by 8 % lower in the proposed model, whereas the carbon atom is more strongly affected. The dipole moment of the nitrile group decreases from 3.859 D in AN to 3.010 D in HCN. Although this change is not negligible, the presented results demonstrate that the charge distribution within the nitrogen atom, which interacts with the alkali cation, and the properties of the C–N bond do not significantly differ between the two species, so we used HCN molecules as explicit solvent molecules for quantum chemical analysis of alkali ion–crown interaction. Note that Pasgreata et al. also used HCN molecules instead of AN for studying coordination of Li^+ in acetonitrile [84].

As cation's desolvation is a process that precedes ion-crown complex formation and significantly affects ion-crown binding energies [85], it is important to establish the number of solvent molecules that surround the two cations in bulk solvent. Coordination number of Na^+ in acetonitrile is estimated to be between 6 and 8 (6[86–88], 6.4[89], 6.8[90], 8.2[91]), whereas according to Thomas et al. K^+ atoms have eight AN molecules in the first solvation shell[87]. Recently, Page and coworkers[92] provided a repository of solvated ions in selected solvents. By analyzing simulations of the two cations with 64 acetonitrile molecules (a link to the corresponding trajectories is given in reference [92]) with the TRAVIS program[93,94], we determined that coordination numbers of Na^+ and K^+ amount to 5.7 and 7.6, respectively. According to these simulations, the sodium/potassium ion is roughly surrounded with

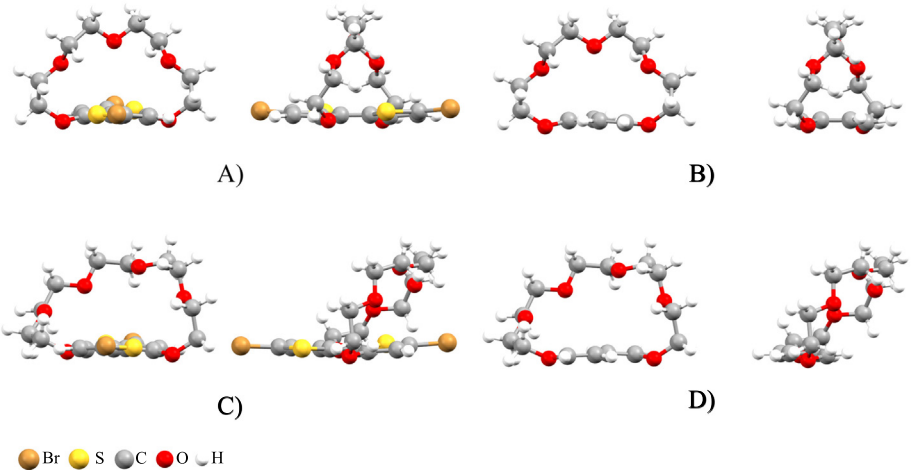

Fig. 1. Decorated crown ethers and crown models used in this work (top and side view): (A) crown 17C5T2 (optimized structure), (B) model M17C5C2 (initial structure), (C) crown 20C6T2 (optimized structure), D) model M20C6C2 (initial structure).

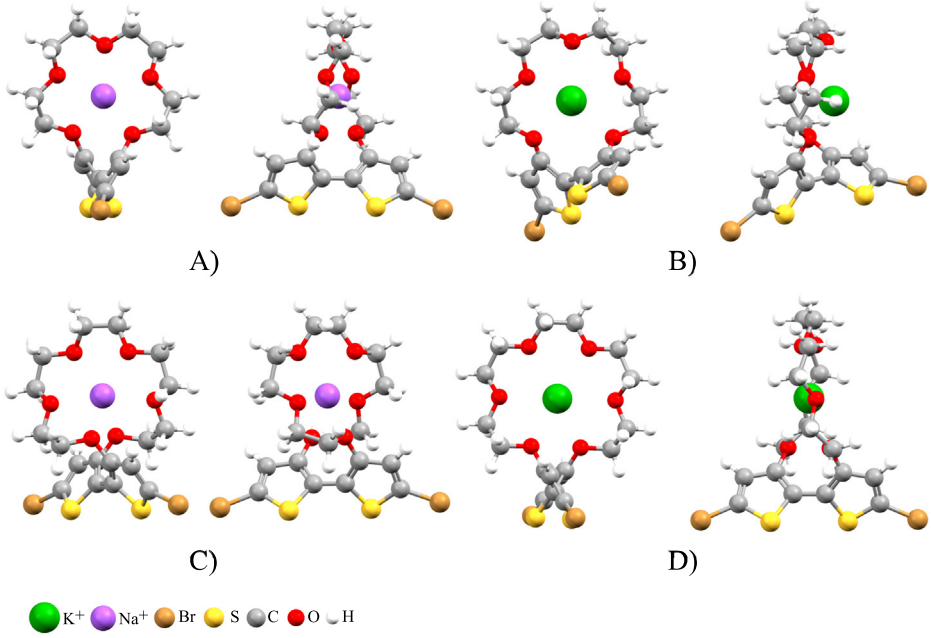

Fig. 2. Optimized structures of four complexes in the gas phase (top and side view): (A) $[17C5T2Na]^+$, (B) $[17C5T2K]^+$, (C) $[20C6T2Na]^+$, D) $[20C6T2K]^+$.

Table 1
Binding energies (in kcal/mol) computed in vacuum (upper values) and with implicit solvent (lower italic values). The results with explicit solvent molecules are presented with respect to $[Na(HCN)_6]^+$ and $[K(HCN)_8]^+$, Eq. 7.

without explicit solvent molecules		with explicit solvent molecules	
$17C5T2Na^+$	−75.1 *−10.0*	$[17C5T2Na(HCN)_2]^+$	−1.0 *−4.4*
$17C5T2K^+$	−55.0 *−10.6*	$[17C5T2K(HCN)_4]^+$	−4.0 *−4.7*
$20C6T2Na^+$	−88.3 *−15.2*	$[20C6T2Na(HCN)_2]^+$	−1.2 *−3.7*
$20C6T2K^+$	−68.0 *−17.2*	$[20C6T2K(HCN)_4]^+$	−12.2 *−10.4*

6/8 AN molecules (optimized structures of $[Na(HCN)_6]^+$ and $[K(HCN)_8]^+$ are depicted in Supplementary Information, Figure S1). Larger number of AN molecules around the bulkier cation is not surprising. Namely, the areas of the isodensity surfaces of the two cations (in vacuum) that correspond to the electron density of 0.001 a.u. equal 78.9 and 137.6 a.u. for Na^+ and K^+, respectively – a significantly larger surface of the potassium ion also implies a larger coordination number. This conclusion is in accord with the literature values for the number of water molecules in the first solvation shell in aqueous solutions: sodium atoms are surrounded by 6 water molecules[87,95,96], while authors suggest 6 to 8 H_2O molecules to coordinate potassium ions (6–7[96], 8[87]). The simulations with 64 water molecules from the above mentioned repository (reference [92]) yield water coordination numbers 6.4 and 10.2 for Na^+ and K^+, respectively. Note that (*i*) the number of solvent molecules around a certain ion depends on the solvent, and (*ii*) the coordination number for potassium cation is larger compared to its smaller counterpart, regardless of the solvent.

A larger coordination number for K^+ compared to Na^+ was also noticed in biological systems and was discussed by several authors.

Table 2
Intra-atomic dipole moments (μ_{intra}^{atom}) and total atomic dipole moments (μ_{total}^{atom}) in AN/HCN. All values are presented in Debye. The dipole moments of the nitrile group in AN and HCN amount to 3.859 and 3.010 D, respectively.

	μ_{intra}^{atom}	μ_{total}^{atom}
N	1.325/ 1.372	2.940/ 2.708
C	2.434/ 2.589	0.920/ 0.301

[97,98,85,99] There is even an experimental proof of the potassium ion being coordinated with as much as nine atoms: Doxsee et al. [100] analyzed the crystal structure of $[(18C6)K(H_2O)_3](H_3O)(H_2O)Cl_2$ obtained by dissolving a crown ether with six oxygen atoms (18C6) in $CHCl_3$ (CH_2Cl_2) in the presence of dipotassium tartarate. In addition to the six crown oxygen atoms, K^+ was here coordinated with three water O atoms. This result confirms the tendency of the potassium ion to coordinate with a larger number of electronegative atoms compared to its analogue with a smaller atomic number. It is also in accord with the Ligand Close Packing Model (LCP) introduced by Gillespie. [101] According to the LCP model, complex geometry is governed by ligand–ligand repulsion: a larger number of surrounding solvent molecules would cause their closer packing and more pronounced repulsion between them, as all AN (HCN) molecules are oriented with their nitrogen atoms towards the alkali cation. Consequently, the ion with smaller surface and volume has a smaller coordination number.

In order to estimate the number of solvent molecules that coordinate the two ions trapped by the studied crown ethers, we performed DFT-MD simulations with a GGA functional by placing the (crown model)–ion complexes in rectangular cells and surrounding them with AN molecules (the computational details are given in Section 2). Crown models M17C5C2 and M20C6C2 were used instead of the crown ethers 17C5T2 and 20C6T2 for the purpose of decreasing the computational effort: the bithiophene units were replaced with CH = CH-CH = CH chains (two carbon chains, label C2), thus keeping the same number of C atoms and CC double bonds. These models are depicted in Fig. 1 and Figure S2 in the Supplementary Information (note that the initial and the optimized structures do not significantly differ). Representative complex geometries from DFT-MD simulations are depicted in Figure S3 in the Supplementary material, while ion–oxygen and ion–nitrogen radial distribution functions are shown in Figures S4 and S5 (the curves are not smooth due to the short simulation time). Note that both ions in both model crowns are coordinated with all oxygen atoms, whereas the number of closest nitrogen atoms helped us to determine how many solvent molecules to employ in the reduced solvation model.

Let us analyze each of the four structures (snapshots from DFT-MD simulations are provided in the Supporting Information, Figure S3):

- The M17C5C2 model is not significantly twisted after capturing Na^+: the sodium ion is basically located in the ring's center and is thus coordinated with all five oxygen atoms, as well as with a single AN molecule on both sides of the crown. As Na^+ is located in the center of 17C5T2 as well, we placed a single HCN molecule on both sides of the ring and created an initial structure for further geometry optimization of the decorated crown ether with a cation and its closest solvent neighbors.
- The potassium cation in $M17C5C2K^+$ is also coordinated with all five O atoms. However, the ion is located outside the crown, as it doesn't fit into the crown's ring, and is solvated with three AN molecules on one side of M17C5C2. The ring is deformed during complexation, and it prevents acetonitrile molecules from approaching the cation from the other side of the ring. As the crown is more rigid than the model (compare Figs. 2 B and S2 B), it is to be expected that the cation might interact with a single AN molecule *through* the M17C5C2 ring. We thus performed optimization of a solvated complex by positioning three solvent molecules close to the cation, and one HCN molecule on the other side of the ring.
- Unlike the 20C6T2 crown, the M20C6C2 model twists while trying to wrap the Na^+ particle in order to provide interaction with all six oxygen atoms, allowing a single AN molecule to approach the ion. As Na^+ is located in the center of 20C6T2, we assumed that one solvent molecule can get close to it on both sides of the ring.
- M20C6C2 also tries to enable coordination of K^+ with all six O atoms. Since the model is more flexible than the crown 20C6T2, it gets deformed and the cation is placed outside the ring, allowing solvent molecules to approach it only from the side which is not protected by the ring. During the simulation, the number of coordinated solvent molecules changes between two and three. On the other hand, K^+ is located at the center of 20C6T2, so we placed two HCN molecules on each side of the ring.

The optimized crown–ion complexes with solvent molecules that interact with the cations are presented in Fig. 3. All optimized structures considered in this manuscript represent minima on the potential energy surfaces. Those structures might not correspond to the global minima on the corresponding potential energy landscapes. Additionally, small atom displacements on rather flat potential surfaces are not energetically demanding and the four clusters are quite flexible. Nevertheless, they provide information we are interested in – getting an insight into solvent's influence on crown–ion interaction, as well as the nature of ion–solvent and crown-solvent interaction.

Optimization of the four complexes with explicit solvent molecules was performed both in the gas phase and in implicit solvent. The binding energies E_{bind} of the solvated complexes were computed by taking into account the energy required to perform desolvation, according to:

$$E_{bind} = \{E_{[crownMS_m]^+} + (n-m)E_S\} - \{E_{crown} + E_{[MS_n]^+}\}. \quad (7)$$

In the above Equation n equals 6 and 8 for sodium and potassium cations, respectively. Label S is used for solvent molecules. Ion-crown complex $[crownM]^+$ is solvated with m HCNs, $[crownMS_m]^+$. The results are presented in Table 1. Neglecting the solvent results in both crowns favoring Na^+, whereas inclusion of explicit solvent molecules that directly interact with the cations forces both crowns to prefer K^+, even when implicit solvation is taken into account.

The computed binding energies are not in accord with experimentally determined crowns' selectivity. However, these structures enable analysis of the nature and the strength of interactions between the three species (the ion, the crown, and the solvent). Let us now turn to the energy decomposition analysis.

3.3. Ion-crown and ion–solvent interaction

The nature of ion-crown and ion–solvent interaction was studied using the Interacting Quantum Atoms approach. The calculations were performed in vacuum, as IQA analysis cannot be performed in conjunction with an implicit solvent. Namely, the PCM model rests on placing the solute in an electric field which depends on the magnitude of solvent molecules' dipole moment. [42] The energy of a charged particle in an electric field is, however,

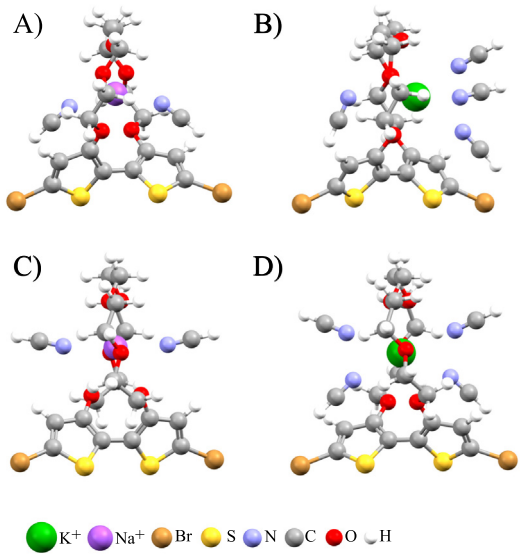

Fig. 3. Optimized structures of four complexes (side view) in the presence of a limited number of explicit solvent molecules: (A) $[17C5T2Na(HCN)_2]^+$, (B) $[17C5T2K(HCN)_4]^+$, (C) $[20C6T2Na(HCN)_2]^+$, (D) $[20C6T2K(HCN)_4]^+$.

gauge dependent, as is thoroughly discussed in reference.[102] Consequently, the gauge is different for each atom, and the total energy does not represent a sum of atomic energies, as required by the IQA methodology.[60,61]

The IQA energy components are summarized in Table 3. We will first analyze the four complexes without solvent molecules. The smaller ring requires the largest amount of energy to accommodate the sodium ion (16.2 kcal/mol), whereas the larger ring needs only 5.5 kcal/mol to integrate the potassium ion. Crown's promotion energy is comparable in all cases and amounts to around 45 kcal/mol. Concerning ion's promotion energy, it is approximately three times larger for K^+. Interestingly, the nature of ion-crown interaction depends on the nature of the cation: the Coulomb term is almost twice the amount of the exchange–correlation energy when Na^+ interacts with either of the two crowns, it is by 34 % larger than E_{xc}^{CK} in $20C6T2K^+$, whereas the two terms are comparable in $17C5T2K^+$. In other words, the larger cation displays a more pronounced non-classical interaction with the host. For both crowns, the overall ion–crown interaction is by roughly 10 kcal/mol stronger with the sodium ion.

The presented results imply that the smaller cation resembles a point-like charge, whereas the larger cation is more polarizable. Indeed, the intra-atomic and total atomic dipole moments of the two alkali ions in the complexes, Table 4, confirm this statement.

Table 4
Intra-atomic dipole moments (μ_{intra}^{atom}) and total atomic dipole moments (μ_{total}^{atom}) of the alkali cations in complexes. All values are presented in Debye.

	μ_{intra}^{atom}	μ_{total}^{atom}
$17C5T2Na^+$	0.003	0.180
$17C5T2Na^+$ with 1 + 1 HCN	0.014	0.272
$17C5T2K^+$	0.295	2.077
$17C5T2K^+$ with 3 + 1 HCN	0.140	0.751
$20C6T2Na^+$	0.006	0.187
$20C6T2Na^+$ with 1 + 1 HCN	0.000	0.106
$20C6T2K^+$	0.014	0.153
$20C6T2K^+$ with 2 + 2 HCN	0.091	0.218

Moreover, the hardness η of the two ions, computed as one half of the difference between the LUMO and the HOMO orbital, amounts to 18.183 and 11.651 eV for Na^+ and K^+ in the gas phase, and 17.127 and 10.890 eV in implicit acetonitrile solvent. The larger hardness is associated with stability and resistance to change [103] as it corresponds to lower polarizability (recent values of Na^+ and K^+ polarizabilities in the gas phase/aqueous solutions are estimated to be 0.157/0.279 and 0.830/0.873 $Å^3$, respectively [104]). In other words, lower hardness of the potassium ion is associated with its larger polarizability and deviation from the spherical shape, as well as stronger non-classical interactions with the crowns.

What a difference a solvent (acetonitrile) makes? Inclusion of explicit solvent molecules weakens ion-crown interaction (the ion–oxygen interaction energies in all eight complexes are tabulated in the Supporting Information, Tables S1 and S2). Both classical and non-classical terms decreased in the 20C6T2 complexes by almost 20 kcal/mol, whereas in the 17C5T2 complexes, the Coulomb and the exchange–correlation term are decreased by approximately 20 and 10 kcal/mol, respectively. The solvent lowers the overall ion-crown interaction energy by up to 40 kcal/mol. Regarding the ion–solvent interaction, in all complexes the Coulomb term is roughly two times larger than the exchange–correlation energy, Table 5. Note that ion–N and ion-O interaction energies are comparable, Table S3. There is only a slight difference in the average ion–solvent energy terms in the solvated complex and in the bulk (Table S4 in the Supplementary Information), and the cations tend to be surrounded with a maximum number of electronegative atoms. Crown–solvent interaction is quite strong, with the dominant non-classical interactions, while the electrostatic interactions are repulsive. Such behavior resembles the collective interaction recently observed by Foroutan-Nejad and coworkers in organometallic systems[105]: although the interaction between the closest atoms is repulsive, the overall interaction between the interacting particles is attractive. Let us consider, for example,

Table 3
IQA energy components (in kcal/mol) for ion-crown interaction: deformation energy (E_{def}), promotion energy (E_{pro}), interaction energy (E_{int}) with its exchange–correlation (E_{xc}) and classical component (E_{cl}). Labels C and M are used for the crown and the metal ion, respectively. Labels $n_1 + n_2$ refer to the number of solvent molecules on each side of the ring.

	E_{def}^{C}	E_{pro}^{C}	E_{pro}^{M}	E_{xc}^{CM}	E_{cl}^{CM}	E_{int}^{CM}	E_{IQA}
$17C5T2Na^+$	16.2	43.3	6.9	−47.0	−94.3	−141.3	−74.9
$17C5T2Na^+$ with 1 + 1 HCN	13.2	51.6	4.3	−36.1	−75.7	−111.8	−108.5
$17C5T2K^+$	11.9	44.3	17.9	−61.4	−68.1	−129.5	−55.3
$17C5T2K^+$ with 3 + 1 HCN	11.6	67.7	20.1	−50.7	−50.4	−101.1	−107.8
$20C6T2Na^+$	10.1	42.7	5.7	−47.6	−106.6	−154.2	−95.7
$20C6T2Na^+$ with 1 + 1 HCN	6.4	44.7	1.2	−30.0	−89.2	−119.2	−116.9
$20C6T2K^+$	5.5	45.0	18.8	−62.1	−82.4	−144.5	−75.2
$20C6T2K^+$ with 2 + 2 HCN	2.8	61.3	15.7	−40.9	−59.4	−100.3	−122.6

Table 5
Overall IQA energy components (in kcal/mol) for ion–solvent interaction: deformation energy (E_{def}), promotion energy (E_{pro}), interaction energy (E_{int}) with its exchange–correlation (E_{xc}) and classical component (E_{cl}). Labels S, M, and C are used for the solvent molecules, the metal ion, and the crown ether, respectively. Labels $n_1 + n_2$ refer to the number of solvent molecules on each side of the ring.

	E^{S}_{def}	E^{S}_{pro}	E^{SM}_{xc}	E^{SM}_{cl}	E^{SM}_{int}	E^{SC}_{xc}	E^{SC}_{cl}	E^{SC}_{int}
with 1 + 1 HCN	0.0	42.5	−14.9	−38.1	−53.0	−67.2	10.9	−56.3
17C5T2K$^+$with 3 + 1 HCN	0.0	71.4	−27.1	−51.2	−78.3	−102.6	6.9	−95.7
20C5T2Na$^+$with 1 + 1 HCN	0.0	33.0	−13.2	−34.8	−48.0	−51.0	16.4	−34.6
20C6T2K$^+$with 2 + 2 HCN	0.0	70.3	−28.2	−54.2	−82.4	−105.9	17.6	−88.3

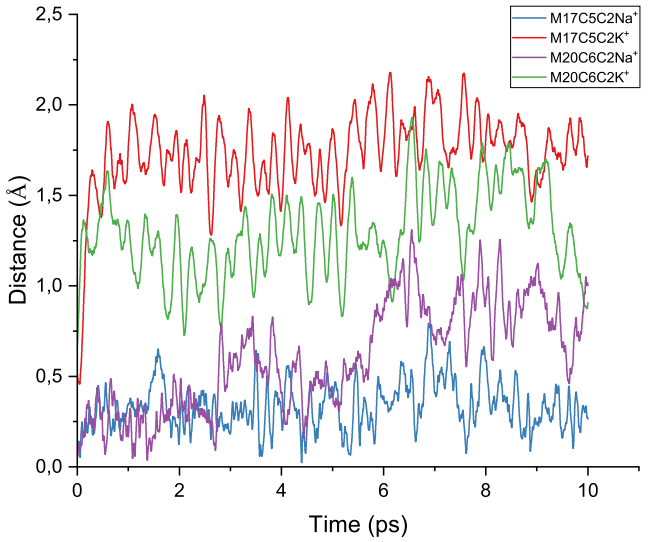

Fig. 4. Time evolution of the distance between the ion and the crown's oxygen atoms' centre of mass.

$[17C5T2Na(AN)_2]^+$. Each of the two nitrogen atoms is the closest to two crown's hydrogen atoms (average distances being 2.73 and 2.79 Å) and one oxygen atom (around 3.14 Å apart). The N-O interactions are repulsive and in both cases amount to 136 kcal/-mol, whereas the N–H interactions are attractive and are estimated to be only between −5 and −6 kcal/mol. Thus, despite the fact that the interaction of solvent's nitrogen atoms with the three closest crown atoms is in total repulsive (which predominantly results from the negative charge located on both N and O), the overall solvent–crown interaction is attractive due to the collective interaction between all the atoms in solvent molecules and all the atoms in the crown.

3.4. Selectivity of the two decorated crown ethers

After analyzing the nature of ion–crown, ion–solvent and crown–solvent interaction, let us address the experimentally determined selectivity of 17C5T2 and 20C6T2. Time evolution of ion-crown distances of the four complexes (distances between the ions and the centers of mass of the crown's oxygen atoms) obtained from DFT-MD simulations is presented in Fig. 4. For the two experimentally observed stable complexes, $[M17C5C2Na]^+$ and $[M20C6C2K]^+$, the ion–crown distances fluctuate around their average values, confirming their stability. The ions in the optimized structures are located in the centers of the corresponding crowns.

The M17C5C2 model lacks the thiophene rings of the real crown, which makes it more flexible than 17C5T2. Consequently, the crown embraces the potassium ion, preventing it from leaving. The 17C5T2 crown, being more rigid, is not able to wrap around K^+ and the ion is located outside the crown. On the other hand, M20C6C2 crown is too spacious for the Na^+ ion, which results in a gradual increase of the Na–crown distance. Average ion–O distances are tabulated in Table 6, and in Tables S5 and S6 in the Supporting information. In the gas phase, average Na^+–O and K^+–O distances do not dependent on the crown. However, explicit solvent molecules introduce a discrepancy of 0.14 Å, bringing the M^+–O distances very close to the M^+–N distances in the microsolvated model. These results demonstrate that ion–solvent interaction is responsible for the low stability of the $[M17C5C2K]^+$ and $[M20C6C2Na]^+$ complexes, and consequently for the pronounced selectivity of the two studied crown ethers towards Na^+ and K^+ ions.

The presented simulations with fixed charges and polarizabilities were sufficient to demonstrate that the solvent molecules have a decisive role in the selectivity of the two studied crown ethers towards Na^+ and K^+ ions. Nevertheless, employment of models that rigorously treat charge and polarization fluxes would result in a more realistic dynamics, which is important when a direct comparison with experiments is sought.

4. Conclusions

Optimal concentration of Na^+ and K^+ is essential for normal functioning of the human body, which prompts their precise determination in blood samples. In this contribution we performed a theoretical analysis of sodium and potassium ion capture by two decorated crown ethers, 17C5T2 and 20C6T2. This research is motivated by recent experimental findings,[11] according to which the two crown ethers are selective towards Na^+ and K^+.

The nature of ion–crown and ion–solvent interaction was studied using the Interacting Quantum Atoms methodology. The dom-

Table 6
Average ion–(crown's oxygen) distances in complexes with and without solvent molecules, and average ion–(solvent's nitrogen) distances in microsolvated models. All values are reported in Å.

$[17C5T2Na]^+$	2.332	$[17C5T2K]^+$	2.697
$[20C6T2Na]^+$	2.393	$[20C6T2K]^+$	2.729
$[17C5T2Na(HCN)_2]^+$	**2.427**	$[17C5T2K(HCN)_4]^+$	2.752
$[20C6T2Na(HCN)_2]^+$	2.565	$[20C6T2K(HCN)_4]^+$	**2.892**
$[Na(HCN)_6]^+$	**2.442**	$[K(HCN)_8]^+$	**2.886**

inant sodium–crown interaction is electrostatic, whereas the non-classical interaction plays a significant role in potassium–crown complexes. Solvent molecules weaken the ion–crown binding when coordinating the metal ion. Na^+ and K^+ are located close to the center of the 17C5T2 and 20C6T2 ring, respectively, forming stable complexes with their hosts. The sodium ion is positioned within the 20C6T2 crown as well, but larger Na-O distances trigger the ion to seek a closer contact with the solvent molecules. The potassium ion is too large to fit within the 17C5T2 ring, so its placement outside of the crown also makes it accessible to the solvent molecules. Ion–solvent attraction thus weakens the interaction of the smaller/larger ion with the larger/smaller crown, which results in pronounced selectivity of 17C5T2 and 20C6T2 for Na^+ and K^+, respectively. We demonstrated that the solvent molecules are crucial for 17C5T2 and 20C6T2 preference towards sodium and potassium ions, while in the gas phase both crowns tightly bind both alkali ions.

The presented results imply that the capture of larger alkali ions, Rb^+ and Cs^+, would predominantly rely on non-classical interactions, as the two of them are significantly softer and thus polarizable (their gas phase polarizabilities are estimated to be 1.370 and 2.360 $Å^3$, respectively[104]). It is to be expected that the same trend follows in the group of the earth alkaline ions (contribution of electrostatic interactions most likely gets smaller as the atomic number gets larger), whereas stronger M^{2+}–solvent interactions might result in even more pronounced selectivity of the corresponding crown ethers. However, the presented results are not sufficient to compare the behavior of the alkaline and the earth alkaline ions in the presence of crown ethers.

CRediT authorship contribution statement

Marijana Hercigonja: Investigation. Visualization. Writing - review & editing. **Branislav Milovanović**: Investigation. Visualization. Writing - review & editing. **Mihajlo Etinski**: Conceptualization. Writing - review & editing. **Milena Petković**: Supervision. Conceptualization. Writing - original draft. Writing - review & editing.

Data availability

Data will be made available on request.

Declaration of Competing Interest

The authors declare that they have no known competing financial interests or personal relationships that could have appeared to influence the work reported in this paper.

Acknowledgment

This work was financially supported by the Ministry Science, Technological Development and Innovation of the Republic of Serbia within the framework of contract number: 451–03-47/2023–01/200146.

Appendix A. Supplementary material

Supplementary data associated with this article can be found, in the online version, at https://doi.org/10.1016/j.molliq.2023.121791.

References

[1] R. Milo, R. Phillips, Cell Biology by the Numbers, Garland Science, 2015.
[2] O.S. Andersen, Cellular Electrolyte Metabolism, in: R.H. Kretsinger, V.N. Uversky, E.A. Permyakov (Eds.), Encyclopedia of Metalloproteins, Springer, 2013, pp. 580–587.
[3] M.A. Zoroddu, J. Aaseth, G. Crisponi, S. Medici, M. Peana, V.M. Nurchi, The essential metals for humans: a brief overview, J. Inorg. Biochem. 195 (2019) 120–129.
[4] P. Lin, F. Yan, H.L.W. Chan, Ion-sensitive properties of organic electrochemical transistors, ACS Appl. Mater. Interfaces 2 (2010) 1637–1641.
[5] P. Lin, F. Yan, Organic thin-film transistors for chemical and biological sensing, Adv. Mater. 24 (2012) 34–51.
[6] S. Wustoni, C. Combe, D. Ohayon, M.H. Akhtar, I. McCulloch, S. Inal, Membrane-free detection of metal cations with an organic electrochemical transistor, Adv. Funct. Mater. 29 (2019) 1904403.
[7] A.-P. Chiriac, M.-D. Damaceanu, A novel approach towards crown-ether modified polyimides with affinity for alkali metal ions recognition, J. Mol. Liq. 322 (2021) 114929.
[8] A.P. de Silva, S.A. de Silva, Fluorescent signalling crown ethers; 'switching on' of fluorescence by alkali metal ion recognition and binding in situ, J. Chem. Soc., Chem. Commun. (1986) 1709–1710.
[9] E. Bakker, M. Lerchi, T. Rosatzin, B. Rusterholz, W. Simon, Synthesis and characterization of neutral hydrogen ion-selective chromoionophores for use in bulk optodes, Anal. Chim. Acta 278 (1993) 211–225.
[10] H. Sakamoto, T. Anase, H. Osuga, K. Kimura, Complexation and fluorescence behavior of a copolymer bearing azacrown ether and anthracene moities, React. Funct. Polym. 71 (2011) 569–573.
[11] A. Giovannitti, C.B. Nielsen, J. Rivnay, M. Kirkus, D.J. Harkin, A.J.P. White, H. Sirringhaus, G.G. Malliaras, I. McCulloch, Sodium and potassium ion selective conjugated polymers for optical ion detection in solution and solid state, Adv. Funct. Mater. 26 (2016) 514–523.
[12] J. Li, D. Yim, W.-D. Jang, J. Yoon, Recent progress in the design and applications of fluorescence probes containing crown ethers, Chem. Soc. Rev. 46 (2017) 2437–2458.
[13] A.T. Harootunian, J.P.Y. Kao, B.K. Eckert, R.Y. Tsien, Fluorescence ratio imaging of cytosolic free Na^+ in individual fibroblasts and lymphocytes, J. Biol. Chem. 264 (1989) 19458–19467.
[14] V.S. Le, B. Kim, W. Lee, J.-E. Jeong, R. Yang, H.Y. Woo, Ratiometric fluorescent ion detection in water with high sensitivity via aggregation-mediated fluorescence resonance energy transfer using a conjugated polyelectrolyte as an optical platform, Macromol. Rapid Commun. 34 (2013) 772–778.
[15] M. Taki, H. Ogasawara, H. Osaki, A. Fukazawa, Y. Sato, K. Ogasawara, T. Higashiyama, S. Yamaguchi, A red-emitting ratiometric fluorescent probe based on a benzophosphole *P*-oxide scaffold for the detection of intracellular sodium ions, Chem. Commun. 51 (2015) 11880–11883.
[16] M. Moser, K.J. Thorley, F. Moruzzi, J.F. Ponder Jr., I.P. Maria, A. Giovannitti, S. Inal, I. McCulloch, Highly selective chromoionophores for ratiometric Na^+ sensing based on an oligoethyleneglycol bridged bithiophene detection unit, J. Mater. Chem. C 7 (2019) 5359–5365.
[17] Z.S. Parr, C.B. Nielsen, Conjugated molecules for colourimetric and fluorimetric sensing of sodium and potassium, Mater. Chem. Front. 4 (2020) 2370–2377.
[18] Y.L. Pak, Y. Wang, Q. Xu, Conjugated polymer based fluorescent probes for metal ions, Coord. Chem. Rev. 433 (2021) 213745.
[19] C.J. Pedersen, Cyclic polyethers and their complexes with metal salts, J. Am. Chem. Soc. 89 (1967) 2495–2496.
[20] U. Tunca, Y. Yagci, Crown ether-containing polymers, Prog. Polym. Sci. 19 (1994) 233–286.
[21] G.W. Gokel, W.M. Leevy, M.E. Weber, Crown ethers: sensors for ions and molecular scaffolds for materials and biological models, Chem. Rev. 104 (2004) 2723–2750.
[22] S.K. Kim, G.I. Vargas-Zúñiga, B.P. Hay, N.J. Young, L.H. Delmau, C. Masselin, C.-H. Lee, J.S. Kim, V.M. Lynch, B.A. Moyer, J.L. Sessler, Controlling cesium cation recognition via cation metathesis within an ion pair receptor, J. Am. Chem. Soc. 134 (2012) 1782–1792.
[23] M. Sundararajan, V. Sinha, T. Bandyopadhyay, S.K. Ghosh, Can functionalized cucurbituril bind actinyl cations efficiently? A density functional theory based investigation, J. Phys. Chem. A 116 (2012) 4388–4395.
[24] S.P. Gromov, S.N. Dmitrieva, A.I. Vedernikov, N.A. Kurchavov, L.G. Kuz'mina, S. K. Sazonov, Y.A. Strelenko, M.V. Alfimov, J.A.K. Howard, E.N. Ushakov, Synthesis, structure, and characterization of chromo(fluoro)ionophores with cation-triggered emission based on *N*-methylaza-crown-ether styryl dyes, J. Org. Chem. 78 (2013) 9834–9847.
[25] M. Dagdevren, I. Yilmaz, B. Yucel, M. Emirik, A novel ferrocenyl naphthoquinone fused crown ether as a multisensor for water determination in acetonitrile and selective cation binding, J. Phys. Chem. B 119 (2015) 12464–12479.
[26] S. Yang, Y. Liu, J. Liao, H. Liu, Y. Jiang, B. Van der Bruggen, J. Shen, C. Gao, Codeposition modification of cation exchange membranes with dopamine and crown ether to achieve high K^+ electrodialysis selectivity, ACS Appl. Mater. Interfaces 11 (2019) 17730–17741.
[27] D. Zhou, M. Zhang, Y. Ma, S. Mukherjee, J. Liu, H. Bian, Cationic effects on the structural dynamics of the metal ion-crown ether complexes investigated by ultrafast infrared spectroscopy, J. Phys. Chem. B 125 (2021) 12797–12805.
[28] L. Fabbrizzi, The origins of the coordination chemistry of alkali metal ions, ChemTexts 6 (2020) 10.
[29] K. Kobiro, New class of lithium ion selective crown ethers with bulky decalin subunits, Coord. Chem. Rev. 148 (1996) 135–149.

[30] H.K. Frensdorff, Stability constants of cyclic polyether complexes with univalent cations, J. Am. Chem. Soc. 93 (1971) 600–606.
[31] J.D. Rodriguez, J.M. Lisy, Probing ionophore selectivity in argon-tagged hydrated alkali metal ion-crown ether systems, J. Am. Chem. Soc. 133 (2011) 11136–11146.
[32] A. Bey, O. Dreyer, V. Abetz, Thermodynamic analysis of alkali metal complex formation of polymer-bonded crown ether, Phys. Chem. Chem. Phys. 19 (2017) 15924–15932.
[33] M.A. Bush, M.R. Truter, The crystal structures of three alkali-metal complexes with cyclic polyethers, J. Chem. Soc. D 1439–1440 (1970).
[34] K. Ohshimo, X. He, R. Ito, F. Misaizu, Conformer separation of dibenzo-crown-ether complexes with Na^+ and K^+ ions studied by cryogenic ion mobility-mass spectrometry, J. Phys. Chem. A 125 (2021) 3718–3725.
[35] M.J. Frisch, G.W. Trucks, H.B. Schlegel, G.E. Scuseria, M.A. Robb, J.R. Cheeseman, G. Scalmani, V. Barone, B. Mennucci, G.A. Petersson, H. Nakatsuji, M. Caricato, X. Li, H.P. Hratchian, A.F. Izmaylov, J. Bloino, G. Zheng, J.L. Sonnenberg, M. Hada, M. Ehara, K. Toyota, R. Fukuda, J. Hasegawa, M. Ishida, T. Nakajima, Y. Honda, O. Kitao, H. Nakai, T. Vreven, J.A. Montgomery, Jr., J.E. Peralta, F. Ogliaro, M. Bearpark, J.J. Heyd, E. Brothers, K.N. Kudin, V.N. Staroverov, T. Keith, R. Kobayashi, J. Normand, K. Raghavachari, A. Rendell, J.C. Burant, S.S. Iyengar, J. Tomasi, M. Cossi, N. Rega, J.M. Millam, M. Klene, J.E. Knox, J.B. Cross, V. Bakken, C. Adamo, J. Jaramillo, R. Gomperts, R.E. Stratmann, O. Yazyev, A.J. Austin, R. Cammi, C. Pomelli, J.W. Ochterski, R.L. Martin, K. Morokuma, V.G. Zakrzewski, G.A. Voth, P. Salvador, J.J. Dannenberg, S. Dapprich, A.D. Daniels, O. Farkas, J.B. Foresman, J.V. Ortiz, J. Cioslowski, D.J. Fox, Gaussian 09 Revision D.01, 2009. Gaussian Inc., Wallingford CT.
[36] Y. Zhao, D.G. Truhlar, The M06 suite of density functionals for main group thermochemistry, thermochemical kinetics, noncovalent interactions, excited states, and transition elements: Two new functionals and systematic testing of four M06-class functionals and 12 other functionals, Theor. Chem. Acc. 120 (2008) 215–241.
[37] A.D. McLean, G.S. Chandler, Contracted Gaussian basis sets for molecular calculations. I. Second row atoms, Z=11-18, J. Chem. Phys. 72 (1980) 5639–5648.
[38] R. Krishnan, J.S. Binkley, R. Seeger, J.A. Pople, Self-consistent molecular orbital methods. XX. A basis set for correlated wave functions, J. Chem. Phys. 72 (1980) 650–654.
[39] T. Clark, J. Chandrasekhar, G.W. Spitznagel, P.v.R. Schleyer, Efficient diffuse function-augmented basis-sets for anion calculations. III. The 3–21+G basis set for first-row elements, Li-F, J. Comp. Chem. 4 (1983) 294–301.
[40] M.J. Frisch, J.A. Pople, J.S. Binkley, Self-consistent molecular orbital methods. 25. supplementary functions for Gaussian basis sets, J. Chem. Phys. 80 (1984) 3265–3269.
[41] J.-P. Blaudeau, M.P. McGrath, L.A. Curtiss, L. Radom, Extension of Gaussian-2 (G2) theory to molecules containing third-row atoms K and Ca, J. Chem. Phys. 107 (1997) 5016–5021.
[42] J. Tomasi, B. Mennucci, R. Cammi, Quantum mechanical continuum solvation models, Chem. Rev. 105 (2005) 2999–3094.
[43] A.D. Becke, Density-functional exchange-energy approximation with correct asymptotic-behavior, Phys. Rev. A 38 (1988) 3098–3100.
[44] C.T. Lee, W.T. Yang, R.G. Parr, Development of the Coll-Salvetti correlation-energy formula into a functional of the electron-density, Phys. Rev. B 37 (1988) 785–789.
[45] S. Grimme, J. Antony, S. Ehrlich, H. Krieg, A consistent and accurate ab initio parametrization of density functional dispersion correction (DFT-D) for the 94 elements H-Pu, J. Chem. Phys. 132 (2010) 154104.
[46] G. Lippert, J. Hutter, M. Parrinello, A hybrid Gaussian and plane wave density functional scheme, Mol. Phys. 92 (1997) 477–488.
[47] J. VandeVondele, J. Hutter, Gaussian basis sets for accurate calculations on molecular systems in gas and condensed phases, J. Chem. Phys. 127 (2007) 114105.
[48] S. Goedecker, M. Teter, J. Hutter, Separable dual-space Gaussian pseudopotentials, Phys. Rev. B 54 (1996) 1703–1710.
[49] G. Bussi, D. Donadio, M. Parrinello, Canonical sampling through velocity rescaling, J. Chem. Phys. 126 (2007) 014101.
[50] D.A. Case, K. Belfon, I.Y. Ben-Shalom, S.R. Brozell, D.S. Cerutti, T.E.I. Cheatham, V.W.D. Cruzeiro, T.A. Darden, R.E. Duke, G. Giambasu, M.K. Gilson, H. Gohlke, A.W. Goetz, R. Harris, S. Izadi, S.A. Izmailov, K. Kasavajhala, A. Kovalenko, R. Krasny, T. Kurtzman, T.S. Lee, S. LeGrand, P. Li, C. Lin, J. Liu, T. Luchko, R. Luo, V. Man, K.M. Merz, Y. Miao, O. Mikhailovskii, G. Monard, H. Nguyen, A. Onufriev, F. Pan, S. Pantano, R. Qi, D.R. Roe, A. Roitberg, C. Sagui, S. Schott-Verdugo, J. Shen, C. Simmerling, N.R. Skrynnikov, J. Smith, J. Swails, R.C. Walker, J. Wang, L. Wilson, R.M. Wolf, X. Wu, Y. Xiong, Y. Xue, D.M. York, P.A. Kollman, AMBER 2020, 2020. University of California, San Francisco.
[51] X. He, V.H. Man, W. Yang, T.-S. Lee, J. Wang, A fast and high-quality charge model for the next generation general AMBER force field, J. Chem. Phys. 153 (2020) 114502.
[52] X. Grabuleda, C. Jaime, P.A. Kollman, Molecular dynamics simulation studies of liquid acetonitrile: New six-site model, J. Comp. Chem. 21 (2000) 901–908.
[53] J. VandeVondele, M. Krack, F. Mohamed, M. Parrinello, T. Chassaing, J. Hutter, QUICKSTEP: Fast and accurate density functional calculations using a mixed Gaussian and plane waves approach, Comp. Phys. Comm. 167 (2005) 103–128.
[54] A.T. Hagler, Force field development phase II: Relaxation of physics-based criteria... or inclusion of more rigorous physics into the representation of molecular energetics, J. Comput. Aided Mol. Des. 33 (2019) 205–264.
[55] C. Liu, J.-P. Piquemal, P. Ren, Implementation of geometry-dependent charge flux into the polarizable AMOEBA+ potential, J. Phys. Chem. Lett. 11 (2020) 419–426.
[56] K. Palmo, B. Mannfors, N.G. Mirkin, S. Krimm, Inclusion of charge and polarizability fluxes provides needed physical accuracy in molecular mechanics force fields, Chem. Phys. Lett. 429 (2006) 628–632.
[57] E. Sedghamiz, B. Nagy, F. Jensen, Probing the importance of charge flux in force field modeling, J. Chem. Theory Comput. 13 (2017) 3715–3721.
[58] Z.E. Hughes, E. Ren, J.C.R. Thacker, B.C.B. Symons, A.F. Silva, P.L.A. Popelier, A FFLUX water model: Flexible, polarizable and with a multipolar description of electrostatics, J. Comput. Chem. 41 (2020) 619–628.
[59] B.C.B. Symons, M.K. Bane, P.L.A. Popelier, DL_FFLUX: A parallel, quantum chemical topology force field, J. Chem. Theory Comput. 17 (2021) 7043–7055.
[60] M.A. Blanco, Á. Martín Pendás, E. Francisco, Interacting quantum atoms: a correlated energy decomposition scheme based on the quantum theory of atoms in molecules, J. Chem. Theory Comput. 1 (2005) 1096–1109.
[61] Á. Martín Pendás, M.A. Blanco, E. Francisco, Chemical fragments in real space: definitions, properties, and energetic decompositions, J. Comput. Chem. 28 (2007) 161–184.
[62] R.F.W. Bader, Atoms in Molecules: A Quantum Theory, Oxford University Press, 1990.
[63] R.F.W. Bader, Atoms in molecules, Acc. Chem. Res. 18 (1985) 9–15.
[64] C.F. Matta, R.J. Boyd (Eds.), The Quantum Theory of Atoms in Molecules: From Solid State to DNA and Drug Design, WILEY-VCH, 2007.
[65] P.I. Dem'yanov, P.M. Polestshuk, Forced bonding and QTAIM deficiencies: a case study of the nature of interactions in He@adamantane and the origin of the high metastability, Chem. Eur. J. 19 (2013) 10945–10957.
[66] Z. Badri, C. Foroutan-Nejad, J. Kozelka, R. Marek, On the non-classical contribution in lone-pair-π interaction: IQA perspective, Phys. Chem. Chem. Phys. 17 (2015) 26183–26190.
[67] C. Foroutan-Nejad, Z. Badri, R. Marek, Multi-center covalency: revisiting the nature of anion-π interactions, Phys. Chem. Chem. Phys. 17 (2015) 30670–30679.
[68] J.L. Casalz-Sainz, J.M. Guevara-Vela, E. Francisco, T. Rocha-Rinza, Á. Martín Pendás, Where does electron correlation lie? Some answers from a real space partition, ChemPhysChem 18 (2017) 3553–3561.
[69] I. Petrović, B. Milovanović, M. Etinski, M. Petković, Theoretical scrutinization of nine benzoic acid dimers: stability and energy decomposition analysis, Int. J. Quantum Chem. 119 (2019) e25918.
[70] N. Orangi, K. Eskandari, J.C.R. Thacker, P.L.A. Popelier, Directionality of halogen bonds: an interacting quantum atoms (IQA) and relative energy gradient (REG) study, ChemPhysChem 20 (2019) 1922–1930.
[71] B.C.B. Symons, D.J. Williamson, C.M. Brooks, A.L. Wilson, P.L.A. Popelier, Does the intra-atomic deformation energy of interacting quantum atoms represent steric energy?, ChemistryOpen 8 (2019) 560–570
[72] J.L. Casalz-Sainz, J.M. Guevara-Vela, E. Francisco, T. Rocha-Rinza, Á. Martín Pendás, Efficient implementation of the interacting quantum atoms energy partition of the second-order Møller-Plesset energy, J. Comp. Chem. 41 (2020) 1234–1241.
[73] J.M. Guevara-Vela, E. Francisco, T. Rocha-Rinza, Á. Martín Pendás, Interacting quantum atoms - a review, Molecules 25 (2020) 4028.
[74] B. Milovanović, A. Stanojević, M. Etinski, M. Petković, Intriguing intermolecular interplay in guanine quartet complexes with alkali and alkaline earth cations, J. Phys. Chem. B 124 (2020) 3002–3014.
[75] B.J.R. Cuyacot, I. Durník, C. Foroutan-Nejad, R. Marek, Anatomy of base pairing in DNA by interacting quantum atoms, J. Chem. Inf. Model. 61 (2021) 211–222.
[76] J.M. Guevara-Vela, M. Gallegos, M.A. Valentín-Rodríguez, A. Costales, T. Rocha-Rinza, Á. Martín Pendás, On the relationship between hydrogen bond strength and the formation energy in resonance-assisted hydrogen bonds, Molecules 26 (2021) 4196.
[77] F. Jiménez-Grávalos, M. Gallegos, Á. Martín Pendás, A.S. Novikov, Challenging the electrostatic σ-hole picture of halogen bonding using minimal models and the interacting quantum atoms approach, J. Comput. Chem. 42 (2021) 676–687.
[78] L.J. Duarte, W.E. Richter, R.E. Bruns, P.L.A. Popelier, Electrostatics explains the reverse Lewis acidity of BH_3 and boron trihalides: infrared intensities and a relative energy gradient (REG) analysis of IQA energies, J. Phys. Chem. A 125 (2021) 8615–8625.
[79] A. Stanojević, B. Milovanović, I. Stanković, M. Etinski, M. Petković, The significance of the metal cation in guanine-quartet – metalloporphyrin complexes, Phys. Chem. Chem. Phys. 23 (2021) 574–584.
[80] P.L.A. Popelier, Non-covalent interactions from a quantum chemical topology perspective, J. Mol. Model. 28 (2022) 76.
[81] N. Pavković, B. Milovanović, A. Stanojević, M. Etinski, M. Petković, Proton leap: shuttling of protons onto benzonitrile, Phys. Chem. Chem. Phys. 24 (2022) 3958–3969.
[82] T.A. Keith, AIMAll (version 19.10.12, professional), 2019. TK Gristmill Software, Overland Park KS, USA, (aim.tkgristmill.com).
[83] R.F.W. Bader, A. Larouche, C. Gatti, M.T. Carroll, P.J. MacDougall, K.B. Wiberg, Properties of atoms in molecules: Dipole moments and transferability of properties, J. Chem. Phys. 87 (1987) 1142–1152.

[84] E. Pasgreta, R. Puchta, A. Zahl, R. van Eldik, Ligand-exchange processes on solvated lithium cations: Acetonitrile and hydrogen cyanide, Eur. J. Inorg. Chem. (2007) 1815–1822.
[85] S. Varma, S.B. Rempe, Structural transitions in ion coordination driven by changes in competition for ligand binding, J. Am. Chem. Soc. 130 (2008) 15405–15419.
[86] D. Spångberg, K. Hermansson, The solvation of Li^+ and Na^+ in acetonitrile from ab initio-derived many-body ion-solvent potentials, Chem. Phys. 300 (2004) 165–176.
[87] M. Thomas, D. Jayatilaka, B. Corry, The predominant role of coordination number in potassium channel selectivity, Biophys. J. 93 (2007) 2635–2643.
[88] S. Nigam, C. Majumder, Microsolvation of sodium ion in acetonitrile clusters: Structure and energetic trend by first principle study, J. Mol. Struct. THEOCHEM 907 (2009) 22–28.
[89] E. Guàrdia, R. Pinzón, On the solvation shell of Na^+ and Cl^- ions in acetonitrile: a computer simulation study, J. Mol. Liq. 85 (2000) 33–44.
[90] L. Troxler, G. Wipff, Conformation and dynamics of 18-crown-6, cryptand 222, and their cation complexes in acetonitrile studied by molecular dynamics simulations, J. Am. Chem. Soc. 116 (1994) 1468–1480.
[91] J. Richardi, P.H. Fries, H. Krienke, The solvation of ions in acetonitrile and acetone: A molecular Ornstein-Zernike study, J. Chem. Phys. 108 (1998) 4079–4089.
[92] K.P. Gregory, G.R. Elliott, E.J. Wanless, G.B. Webber, A.J. Page, A quantum chemical molecular dynamics repository of solvated ions, Sci. Data 9 (2022) 430.
[93] M. Brehm, B. Kirchner, TRAVIS - a free analyzer and visualizer for Monte Carlo and molecular dynamics trajectories, J. Chem. Inf. Model. 51 (2011) 2007–2023.
[94] M. Brehm, M. Thomas, S. Gehrke, B. Kirchner, TRAVIS - a free analyzer for trajectories from molecular simulation, J. Chem. Phys. 152 (2020) 164105.
[95] Y.I. Neela, A.S. Mahadevi, G.N. Sastry, First principles study and database analyses of structural preferences for sodium ion (Na^+) solvation and coordination, Struct. Chem. 24 (2013) 67–79.
[96] Y. Chen, Y. Zhu, Y. Ruan, N. Zhao, W. Liu, W. Zhuang, X. Lu, Molecular insights into multilayer 18-crown-6-like graphene nanopores for K^+/Na^+ separation: a molecular dynamics study, Carbon 144 (2019) 32–42.
[97] S.Y. Noskov, S. Bernèche, B. Roux, Control of ion selectivity in potassium channels by electrostatic and dynamic properties of carbonyl lygands, Nature 431 (2004) 830–834.
[98] S. Varma, S.B. Rempe, Tuning ion coordination architectures to enable selective partitioning, Biophys. J. 93 (2007) 1093–1099.
[99] M.I. Chaudhari, J.M. Vanegas, L.R. Pratt, A. Muralidharan, S.B. Rempe, Hydration mimicry by membrane ion channels, Annu. Rev. Phys. Chem. 71 (2020) 461–484.
[100] K.M. Doxsee, H.R. Wierman, T.J.R. Weakley, Unusual coordination number and geometry in a potassium 18-crown-6 complex, J. Am. Chem. Soc. 114 (1992) 5165–5171.
[101] R.J. Gillespie, P.L.A.P. Eds, Chemical Bonding and Molecular Geometry: From Lewis to Electron Densities, Oxford University Press, New York, 2001.
[102] C. Foroutan-Nejad, R. Marek, Potential energy surface and binding energy in the presence of an external electric field: Modulation of anion-π interactions for graphene-based receptors, Phys. Chem. Chem. Phys. 16 (2014) 2508–2514.
[103] T.K. Ghanty, S.K. Ghosh, A density functional approach to hardness, polarizability, and valency of molecules in chemical reactions, J. Phys. Chem. 100 (1996) 12295–12298.
[104] M. Li, B. Zhuang, Y. Lu, Z.-G. Wang, L. An, Accurate determination of ion polarizabilities in aqueous solutions, J. Phys. Chem. B 121 (2017) 6416–6424.
[105] S. Sowlati-Hashjin, V. Šadek, S.A. Sadjadi, M. Karttunen, Á. Martín Pendás, C. Foroutan-Nejad, Collective interactions among organometallics are exotic bonds hidden on lab shelves, Nat. Commun 13 (2022) 2069.